Stem Cell Research & Therapy

RESEARCH

Open Access

# AGEs impair osteogenesis in orthodontic force-induced periodontal ligament stem cells through the KDM6B/Wnt self-reinforcing loop

Qiaohui Ying[1,2,3], Yujun Jiang[1,2], Changyun Sun[1,2,3], Yaoguang Zhang[1,2,3], Ruihan Gao[1,2], Hongrui Liu[1,2,3], Hongrui Liu[1,2,4*], Jie Guo[1,2,3*] and Minqi Li[1,2,5*]

## Abstract

**Background** Diabetes, occasionally diagnosed in orthodontic patients, can impede orthodontic tooth movement (OTM) by accumulating advanced glycation end products (AGEs) in the periodontium. This accumulation impairs the osteogenic differentiation of periodontal ligament stem cells (PDLSCs) due to alterations in the force-loaded microenvironment, yet the underlying mechanisms remain elusive.

**Methods** Bioinformatics analysis of GSE112122 identified alterations in the mechanical regulation of histone methylation enzyme Lysine Demethylase 6B (KDM6B). OTM models were established in healthy and Nicotinamide/Streptozotocin-induced type II diabetic rats. The impact of AGEs on mechanically induced osteogenesis and its correlation with KDM6B were evaluated by assessing the therapeutic effects of periodontal ligament injections of the AGEs/RAGE inhibitor FPS-ZM1. To investigate transcriptomic changes, we extracted human PDLSCs, which were subjected to RNA sequencing following the overexpression of KDM6B. Experimental validation further identified potential self-reinforcing loops and their associated antioxidative mechanisms.

**Results** Mechanical forces upregulated KDM6B expression and function in PDLSCs, modulating extensive downstream osteogenesis-related transcriptional changes. Experiments with AGEs-treated and FPS-ZM1-treated samples demonstrated that AGEs impaired osteogenesis by compromising KDM6B mechanical responsiveness. A positive feedback loop between KDM6B and Wnt pathways was identified, inhibited by AGEs. This loop regulated superoxide dismutase 2 (SOD2), facilitating antioxidative stress and preventing stem cell ageing.

**Conclusions** This study elucidates a novel mechanism by which AGEs influence the osteogenic process and antioxidative capacity of PDLSCs through the KDM6B/Wnt self-reinforcing loop under orthodontic force. Targeting the AGE/RAGE pathway or enhancing KDM6B may enhance orthodontic treatments for diabetic patients.

*Correspondence:
Hongrui Liu
yf1blhr@126.com
Jie Guo
kqgj@sdu.edu.cn
Minqi Li
liminqi@sdu.edu.cn

Full list of author information is available at the end of the article

**Keywords** Orthodontics, Stem cells, Diabetes mellitus, Histone lysine demethylase, Wnt signalling pathway, Antioxidative stress

## Introduction

Against the rising incidence of malocclusions, adults and children increasingly pursue orthodontic treatments for aesthetic and dental health benefits. However, these treatments pose substantial clinical challenges, especially for individuals with systemic conditions such as diabetes [1]. Periodontal ligament stem cells (PDLSCs) are characterized by self-renewal capability and multipotent differentiation potential [2]. These cells migrate and differentiate into osteoblasts during orthodontic tooth movement (OTM) [3]. However, the functional state of PDLSCs is easily affected by systemic diseases. For example, metabolic changes induced by systemic diseases can impair the functions of PDLSCs, including programmed cell death and osteogenic differentiation [4, 5]. Therefore, exploring the behavioural changes in PDLSCs under mechanical stimulation in the context of systemic diseases is necessary.

Diabetes mellitus, particularly type II diabetes mellitus (T2DM), is a widespread and increasingly severe chronic metabolic disorder affecting both adults and children [6, 7]. Managing T2DM during extended orthodontic treatments is challenging due to the need for consistent glycemic control, which is further complicated by the long-term effects of hyperglycemic memory caused by advanced glycation end products (AGEs) [8]. AGEs are stable polymers produced by nonenzymatic reactions between proteins, lipids, nucleic acids, and glucose [2]. The accumulated AGEs interact with their receptor for advanced glycation end products (RAGE). This interaction induces various intracellular signalling pathways to produce reactive oxygen species (ROS) and reactive nitrogen species, leading to different pathological responses [9]. Additionally, AGEs increase collagen matrix rigidity and hinder the interaction between osteocalcin and osteopontin, enhancing bone fragility [10]. Recent studies have revealed elevated levels of AGEs in the periodontal tissues of T2DM patients during orthodontic treatment [11]. However, research on how AGEs specifically affect OTM remains limited.

Previous research has demonstrated that the hyperglycemic memory induced by AGEs may be attributed to epigenetic mechanisms, which alter gene expression without changing the DNA sequence itself [12]. Among these mechanisms, histone modifications, particularly methylation, are crucial in regulating spatiotemporal expression patterns and heritability [13]. Specifically, histone H3 lysine 27 trimethylation (H3K27Me3), a form of transcriptional repression, is one of the epigenetic barriers observed in dental mesenchymal stem cells [14]. Lysine demethylase 6B (KDM6B), which explicitly targets H3K27Me3 for demethylation, promotes the transcription of osteogenic markers [15]. It can be activated by mechanical forces and Wnt ligands, facilitating Wnt/β-catenin signalling to enhance stem cell differentiation [14, 16]. Recent studies indicate that KDM6B regulates stem cell adaptability and regenerative capacity in inflammatory niches [17]. However, the variations in KDM6B within PDLSCs under orthodontic force and whether it regulates stem cell adaptability to inflammation in the diabetic microenvironment are unclear.

This study aimed to investigate the impact of the diabetic microenvironment, characterized by AGEs, on orthodontic force-induced PDLSCs through histone modifications. Results showed that orthodontic force promoted KDM6B expression and H3K27Me3 demethylation in PDLSCs, but AGEs inhibited this process. Specifically, AGEs impaired osteogenic and antioxidative capabilities by suppressing the KDM6B/Wnt self-reinforcing loop. This study reveals a novel epigenetic mechanism by which AGEs influence mechanically induced osteogenic differentiation of stem cells and suggests that targeting the AGEs receptor or enhancing KDM6B could offer new strategies for improving orthodontic treatment in T2DM patients.

## Methods

### Acquisition and analysis of public data

The Gene Expression Omnibus (GEO, https://www.ncbi.nlm.nih.gov/geo/) is a public genomic database. We acquired the GSE112122 dataset from this database, focusing on analyzing intermittent force groups and their corresponding controls. We conducted differential expression analysis utilizing the DESeq2 package (version 1.42.0), identifying genes as differentially expressed (DEGs) based on $P$ values $<0.05$ and $|\log2\text{-fold change}| > 1$. Additionally, the Cistrome Data Browser (http://cistrome.org/db), a repository of ChIP-seq data for human and mouse genomes, provided data on H3K27Me3 enrichment at gene loci within pluripotent stem cells from GSE1946.

### Construction of OTM and T2DM animal models

The study was approved by Shandong University's Ethical Committee (**No: 20231116**) and followed NIH animal care guidelines. The details are listed in the **ARRIVE guidelines** (Supplementary File 1). We divided the rats into the Control, OTM, T2DM+OTM+nT, T2DM+OTM+FPS-ZM1, and OTM+GSK-J4 groups. Each group was established to consist of five samples, as

determined by the Resource Equation Method (Supplementary File 2) and published literature [18, 19]. The T2DM models were induced with a single dose of STZ (60 mg/kg) following NA pretreatment (120 mg/kg). Successful T2DM induction was verified with post-2-hour glucose levels over 11.1 mmol/L [20, 21]. The OTM models applied a 20 g force using nickel-titanium springs for 14 days, with control rats receiving the device without force. Oral hygiene was rigorously upheld to avert gingivitis, and the stability of orthodontic devices was consistently monitored.

#### Processing of tissue samples

Euthanasia was carried out on the animals by administering an overdose of anesthetic (intraperitoneal injection of 1% pentobarbital at a dosage of 100 mg/kg body weight). Maxillary bones were dissected, and portions of periodontal tissue were harvested for protein extraction for subsequent experiments. The maxillae were fixed in 4% paraformaldehyde (PFA), decalcified at 4 °C with a 10% EDTA-2Na solution for one month, dehydrated in ethanol, and then embedded in paraffin according to standard protocols. Five-micron-thick sections were prepared for histological analysis.

#### Enzyme-linked immunosorbent assay

The concentration of AGEs in periodontal tissue extracts was measured using a Rat AGEs ELISA Kit (JL12657, Jianglai Biotechnology Co., Ltd., China). The kit strips were equilibrated to room temperature for 10 min after storage at 4 °C. The test samples were diluted fivefold, and an HRP-conjugated antibody solution was added to the wells. After one hour of incubation at 37 °C under an adhesive film, the wells were washed five times with a wash buffer. Then, tetramethylbenzidine was added, the mixture was incubated in the dark at 37 °C for 15 min, and the reaction was stopped with 50 µl of stop solution. The optical density was immediately read at 450 nm.

#### Histology and IHC assessment

Sample preparation included dehydration through an ethanol gradient, clearing in xylene, and paraffin embedding. Sections were stained with hematoxylin-eosin (HE) and Masson staining following standard protocols. For IHC, the sections were incubated overnight at 4 °C with primary antibodies against AGER, RUNX2, ALP, Wnt2, and Wnt5A (Supplementary File 3), with IgG used as a negative control, followed by incubation with the corresponding secondary antibodies for one hour at room temperature. Diaminobenzidine (DAB) (Zsbio, Beijing, China) was used to detect immunoreactivity. The sections were then mounted in neutral balsam and analyzed under a BX53 microscope (Olympus). ImageJ software was used for semiquantitative assessment of staining intensity and cell counts.

#### Tissue immunofluorescence for colocalization

Sections were deparaffinized, hydrated, and incubated for 30 min with 0.3% hydrogen peroxide at room temperature to inhibit endogenous peroxidase activity. After blocking with 1% BSA in phosphate-buffered saline (PBS) for one hour, the sections were exposed overnight at 4 °C to a mixture of mouse anti-CD90 and rabbit anti-KDM6B, H3K27Me3, β-catenin (CTNNB1), and CAMK II antibodies (Supplementary File 3). Species-specific fluorescent secondary antibodies were then applied and incubated in the dark at room temperature for one hour. Nuclei were stained with DAPI before mounting. A Leica fluorescence microscope facilitated fluorescence observation, with semiquantitative colocalization analysis via ImageJ focusing on signal overlap suggestive of protein interactions or coexpression.

#### Extraction, purification, and identification of PDLSCs

Five volunteers (18–23 years old) who underwent orthodontic premolar extractions participated with the approval of the Ethics Committee of Shandong University School of Stomatology (**No: 20231115**). Following established protocols [22], periodontal ligament tissue was carefully harvested and sectioned into fragments smaller than 0.125 $mm^3$. The tissue fragments were placed in culture flasks and incubated upside down for five hours to promote adhesion. Subsequently, they were cultured upright in a complete medium (10% FBS, 1% PS, and α-MEM) at 37 °C and 5% $CO_2$ for approximately 4.5 days. Third-generation PDLSCs, derived by limiting dilution, were cultured in osteogenic and adipogenic induction media for 21 days. Osteogenic and adipogenic differentiation were assessed using Alizarin Red and specific adipogenic stains. Flow cytometry for $CD73^+$ (Biolegend, USA), $CD90^+$ (Biolegend, USA), and $CD105^+$ (Biolegend, USA)confirmed the presence of nonhematopoietic stem cells with osteogenic potential, excluding $CD45^-$ (Biolegend, USA) cells.

#### Mechanical loading and drug treatments of PDLSCs

BioFlex® silicone molds were pre-coated with 1.5 mg/mL type I rat tail collagen, and human PDLSCs were seeded at $2.0\times10^5$ cells/well. Following prior research [19], cyclic tension stress (10%, 0.5 Hz) was applied with a Flexcell Tension System (Flexcell 6000) to mimic the stretching forces in orthodontic tooth movement. The effects of AGEs/RAGE on mechanically induced osteogenesis was assessed by introducing exogenous AGEs (Abcam, ab51995) at 200 µg/ml and FPS-ZM1 (MCE, HY-19370) at 10 µM. The role of KDM6B was inhibited with 5 µM GSK-J4 (MCE, HY-15648B). The roles of the canonical

and noncanonical Wnt pathways were probed using LiCl (Beyotime, ST498) at 10 μM, XAV939 (MCE, HY-15147) at 20 μM, KN-93 (Beyotime, SD9536) at 50 nM, and cytochalasin D (MCE, HY-N6682) at 1 μM for 30 min.

#### KDM6B overexpression plasmid transfection in PDLSCs

KDM6B overexpression was achieved with the pcDNA3.1-3xFlag-C vector (NM_000435) from Keyan Cloud Technology, Shandong, China. PDLSCs were seeded at $3\times10^5$ cells/well in six-well plates to adhere. After adhering, the cells were prepared for transfection by culture in serum-free, antibiotic-free α-MEM for 12 h. The transfection mixture was added to the wells, comprising 2 μg of DNA and 10 μl of ZLip2000 (ZOMANBIO, China) in 500 μl of Opti-MEM I. After 6 h at 37 °C in a $CO_2$ incubator, the medium of the cells was replaced with a complete medium, and the cells were incubated for another 24 h. We use qRT-PCR and western blot to analyze mRNA and protein expression, confirming transfection efficacy. Subsequent interventions were applied as necessary, maintaining a coherent experimental progression from setup to analysis.

#### RNA extraction and qRT-PCR

After treatment, h-PDLSCs were washed with PBS, and total RNA was extracted using RNAex Pro RNA extraction reagent (AG21102) per the manufacturer's instructions. Subsequently, mRNA was reverse-transcribed into cDNA using the Evo M-MLV Plus cDNA Synthesis Kit (AG11615). Real-time PCR analysis was performed on an Applied Biosystems 7500 Real-Time PCR System (Life Technologies Corporation, USA) using the FastStart Universal SYBR Green Kit (AG11746) to quantify mRNA expression levels. *ACTB* was used as an internal control, and the $2^{-\Delta\Delta CT}$ method was used to analyze triplicate data. The sequences of the human primers used are detailed in Supplementary File 4.

#### RNA sequencing and data analysis

Twenty-four hours post-transfection with either a control (empty vector) or KDM6B overexpression vector, total RNA was extracted from PDLSCs and sequenced on the Illumina HiSeq 2500 platform (Novogene, China). Transcriptome assembly and read mapping were performed using Trinity and RSEM to ensure accurate transcript quantification. DESeq2 (v1.20.0) was used to normalize gene expression, and DEGs with an FDR < 0.05 and a $|\log2FC| > 1$ were identified. DEGs were organized into heatmaps using K-means clustering (Euclidean distance). The gene ontology (GO), kyoto encyclopedia of genes and genomes (KEGG), and gene set enrichment analysis (GSEA) enrichment analyses were performed using clusterProfiler (v3.8.1), prioritizing significant categories by p-value. The protein-protein interaction (PPI) networks were mapped using the String database (https://string-db.org/).

#### Protein extraction and western blotting

Protein extraction was performed at 4 °C. Cells were washed with PBS and lysed in RIPA buffer (P0013B, Beyotime) supplemented with 1% protease (P1005, Beyotime) and phosphatase inhibitors (HY-K0022, MCE). Nuclear and cytoplasmic proteins were isolated using a Nuclear and Cytoplasmic Protein Extraction Kit (PK10014, Proteintech). Protein concentrations were measured with a BCA kit (P0012, Beyotime). Proteins were separated by electrophoresis on Tris-glycine gels and transferred to PVDF membranes (0.45 μm). The membranes were blocked with 5% BSA in TBST for 1 h, incubated overnight at 4 °C with primary antibodies, and then with HRP-linked secondary antibodies for 1 h at room temperature. Immunoreactive bands were visualized using enhanced chemiluminescence (ECL) substrate. GAPDH or β-actin served as loading controls, and band intensities were quantified using ImageJ (NIH). The antibody details are provided in Supplementary File 5.

#### ALPase staining and quantitative analysis

After 24 h of force application, PDLSCs were washed with PBS and fixed in 4% paraformaldehyde for 20 min. Following the manufacturer's instructions, alkaline phosphatase (ALPase) activity was assessed using a BCIP/NBT Alkaline Phosphatase Color Development Kit (C3206, Beyotime). After 6 h of staining, ALP-positive cells were examined under an Olympus BX-53 microscope (Tokyo, Japan). A phosphatase inhibitor-free lysis buffer was used for protein extraction. ALP activity was quantitatively analyzed with a detection kit (P0321S, Beyotime), and the absorbance was read at 405 nm.

#### Alizarin Red S staining

Following exposure to cyclic mechanical stress (8 h/day for 14 days) under osteogenic induction conditions [23], PDLSCs were subjected to dual PBS washes and fixed in 4% paraformaldehyde for 20 min. The cells were stained with a 0.2% Alizarin Red solution (C0140, Beyotime) for 6 h. After thorough rinsing with PBS, the formation of mineralized nodules was visualized using an Olympus BX-53 light microscope (Tokyo, Japan). This process highlights the osteogenic differentiation potential of PDLSCs by detecting calcium deposit formation, which indicates mineralized matrix production.

#### β-Galactosidase staining during senescence

After washing with PBS, PDLSCs were fixed with β-galactosidase staining fixative at room temperature for 15 min. Following another PBS wash, the cells were covered with a staining working solution (C0602, Beyotime)

according to the manufacturer's instructions and incubated overnight at 37 °C. Subsequently, the cells were washed with 70% ethanol to remove any unbound dye or crystals. Observations were made under an Olympus BX-53 light microscope, and semiquantitative statistical analysis was conducted using ImageJ.

#### Cell immunofluorescence

The cells were fixed in 4% paraformaldehyde for 20 min, washed with PBS, and permeabilized with 0.5% Triton X-100. The sections were blocked in 5% BSA-PBS before they were incubated overnight at 4 °C with primary antibodies. Then, the cells were incubated with fluorophore-conjugated secondary antibodies for 1 h at room temperature. DAPI (ab104139, Abcam) was used for nuclear staining for 5 min. Visualization was performed via a DMi8 Automated Fluorescence Microscope (Leica, Germany), and fluorescence intensity was quantified using ImageJ's mean grey value (MGV). The details of the antibodies used are provided in Supplementary File 3.

#### Detection of intracellular calcium ions

A working solution of Fluo-4 AM (0.5 μM, S1060, Beyotime) was prepared according to the manufacturer's instructions. The culture medium of the PDLSCs was removed, and the cells were washed with PBS. Subsequently, the Fluo-4 AM solution was added to the cells, which were then incubated in the dark at room temperature for 15 min to allow for the loading of the dye into the cells. The fluorescence intensity, indicative of the intracellular calcium ion concentration, was observed directly using a DMi8 automated fluorescence microscope. The peak levels of calcium ion signaling were also quantitatively analyzed using a BD Accuri® C6 flow cytometer.

#### Prediction of transcription factors

The promoter sequence of the KDM6B gene was retrieved from the UCSC Genome Browser database (https://genome.ucsc.edu/). We designated the 2000 nucleotide (nt) region upstream of the transcription start site (TSS) as the promoter region of interest. We used the PROMO database to identify transcription factors associated with canonical and noncanonical Wnt signalling pathways (https://alggen.lsi.upc.edu/recerca/menu_recerca.html). Subsequently, the JASPAR database (https://jaspar.genereg.net/) confirmed the predicted TF binding sites within the selected promoter region.

#### Detecting the formation of cellular tunnelling nanotubes

The cells were fixed in 4% PFA for 20 min and washed in 0.1% Triton X-100 PBS. The sections were blocked with 2% BSA in PBS for 1 h and then incubated with SOD2 primary antibodies at room temperature for two hours, followed by a one-hour incubation with fluorophore-conjugated secondary antibodies (1:200 dilution) and Actin-Tracker in 2% BSA and 0.1% Triton X-100 PBS. DAPI (ab104139, Abcam) was used for 5-minute nuclear staining. An FV3000 laser confocal microscope (Japan) was used for imaging, with Z-stacks captured in 0.4 μm steps by an inverted Zeiss LSM 700 microscope using Zen software. TNT connections, identified by F-actin structures and analyzed through Z-stack scanning, were classified based on the following criteria: (i) no substrate contact, appearing above the first 3–4 Z-stacks; (ii) thickness less than 1 mm; and (iii) a continuous "bridge" between cells. TNT enumeration and SOD2 staining were integrated, highlighting protein transfer as a critical distinction from noncommunicative protrusions such as filopodia [24, 25].

#### Detection of intracellular ROS levels

DCFH-DA (S0033, Beyotime) was used to quantify the cellular ROS levels. After various treatments, the cells were incubated with 10 μmol/L DCFH-DA in α-MEM for 30 min at 37 °C, allowing DCFH-DA to enter the cells and be oxidized by ROS into fluorescent DCF. After incubation, the cells were washed to eliminate residual dye and analyzed under a DMi8 fluorescence microscope (Leica) to measure DCF fluorescence, which indicates the ROS concentration.

#### Statistical analysis

Data analysis was performed using SPSS version 25.0 (SPSS Inc., Armonk, USA), and figures were created with GraphPad Prism 9.0 (GraphPad Software Inc., San Diego, USA). Normally distributed data are shown as the mean ± standard deviation for samples of three or more variables. Two-tailed Student's t-tests were used to assess differences between the two groups, while one-way ANOVA with Tukey's post hoc test was used in three more groups. Nonnormally distributed data were analyzed using nonparametric rank sum tests. $P<0.05$ was considered to indicate statistical significance. This rating system indicates levels of statistical significance based on P values: one asterisk (*) indicates $P<0.05$, two asterisks (**) indicate $P<0.01$, and three asterisks (***) indicate $P<0.001$.

## Results

#### Mechanical force promotes the demethylation of H3K27Me3 and the expression of KDM6B

To determine whether orthodontic force induces changes in histone-modifying enzymes, a bioinformatic analysis of the GSE112122 dataset related to intermittent force was performed. Differential expression analysis identified 2,732 upregulated and 3,036 downregulated genes (Fig. 1a). Enrichment analysis revealed biological mechanisms associated with osteogenesis (Fig. 1b-c).

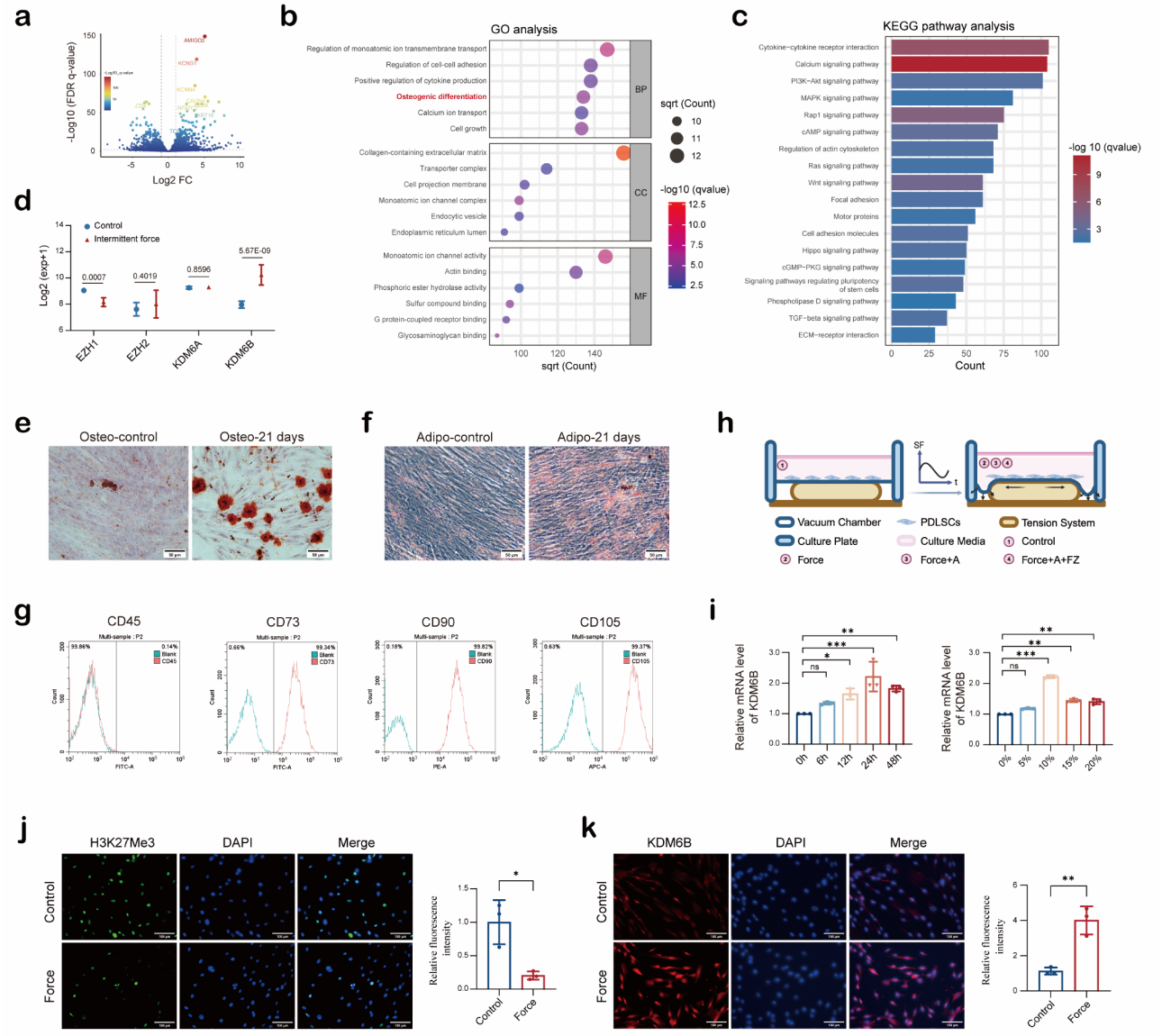


**Fig. 1** Mechanical force promotes the expression of KDM6B and the demethylation of H3K27Me3. (**a**) The volcano plot showed DEGs between the control and intermittent force groups in the GSE112122 dataset. (**b**) GO analysis showing BP, CC, and MF terms. (**c**) KEGG analysis demonstrated pathway enrichment. (**d**) Expression levels of genes related to H3K27Me3-modifying enzymes. (**e**) Alizarin Red staining; scale bar = 50 μm. (**f**) Oil Red O staining; scale bar = 50 μm. (**g**) Flow cytometry was used to analyze PDLSC surface markers. (**h**) Schematic of intermittent force application and grouping. (**i**) The mRNA expression levels of *KDM6B* varied with time and force, as measured by qRT-PCR, $n = 3$. (**j**, **k**) Cell fluorescence was used to measure the number of H3K27Me3- and KDM6B-positive cells; $n = 3$. Data were shown as mean ± SD. Significance: $^{*}P < 0.05$, $^{**}P < 0.01$, $^{***}P < 0.001$

Among the enzymes regulating H3K27me3 modification, KDM6B demonstrated significant mechanical sensitivity (Fig. 1d). Human PDLSCs, which were extracted and confirmed to have multipotent differentiation potential (Fig. 1e-f), expressed mesenchymal stem cell markers CD73, CD90, and CD105 and lacked the hematopoietic stem cell marker CD45 (Fig. 1g). Intermittent stress loading was applied to simulate orthodontic force, with experimental groups based on the schematic diagram (Fig. 1h). Under varying stress conditions, KDM6B mRNA levels were time-dependent and responsive to changes in force magnitude, with the most significant increase observed after 24 h of 10% tension (Fig. 1i). Consequently, 0.5 Hz, 10% tension and 24 h were determined to be the optimal force parameters. Under these conditions, there was a significant promotion of H3K27me3 demethylation and KDM6B expression (Fig. 1j-k).

### KDM6B regulates downstream transcriptional pathways associated with force-induced osteogenic differentiation

Transcriptome sequencing was performed to investigate the role of KDM6B in mechanically induced osteogenic

differentiation following KDM6B overexpression (OE-KDM6B). The differential analysis identified 2,498 upregulated and 1,464 downregulated genes found after OE-KDM6B, as visualized in the volcano plot (Fig. 2a). A clustering heatmap highlighted the top 20 differentially expressed genes, with significant upregulation of osteoglycin (*OGN*) and *COL11A1* (Fig. 2b). Considering the role of type I, III, and VII collagen in periodontal tissue remodelling, and osteogenesis, increased expression of *COL1A1*, *COL1A2*, *COL3A1* and *COL7A1* was detected (Fig. 2c). The intersection of OE-KDM6B overexpressed genes with those from the GSE112122 dataset revealed 290 commonly upregulated genes in response to mechanical force and KDM6B overexpression (Fig. 2d). GO analysis showed activation of biological processes related to osteogenic differentiation (Fig. 2e), while KEGG analysis indicated reactivation of pathways, including Wnt signalling (Fig. 2f). Further analysis using the GSE1946 dataset demonstrated H3K27me3 enrichment on osteogenic factors such as *ALP*, *RUNX2*, *BMP2*, and *COL1A1* in pluripotent stem cells, suggesting that KDM6B-mediated removal of H3K27me3 is critical for osteogenic differentiation (Fig. 2g). The PPI network analysis identified an osteogenesis-related gene cluster centered around *BMP2* and *COL1A1* (Fig. 2h). In *vivo* experiments confirmed that orthodontic force significantly enhanced the activation of osteogenic markers Alp and Runx2 [26, 27], an effect that was inhibited by the KDM6B inhibitor GSK-J4, highlighting the role of KDM6B in osteogenesis (Fig. 2i).

#### AGEs inhibit mechanical force-induced KDM6B expression and its mediated histone demethylation

As shown in the schematic, OTM models were constructed under both healthy and T2DM conditions, with treatment using FPS-ZM1 to highlight the impact of AGEs (Fig. 3a). Successful OTM was indicated by mesial movement and increased distal periodontal ligament width of the first molar (Fig. 3b, Figure S1). The T2DM model exhibited reduced insulin sensitivity (as indicated by IPGTT) and elevated periodontal AGEs' levels (Figure S2-3). Mechanical force increased collagen content and alignment in the periodontal ligament, while the diabetic environment led to collagen degradation, which was improved by FPS-ZM1 injection (Fig. 3c). Histological analysis revealed upregulation of RAGE in the periodontal ligament under diabetic conditions, indicating activation of the AGE/RAGE pathway (Fig. 3d). These results confirmed the successful establishment of animal models.

In *vivo*, immunofluorescence analysis showed that mechanical force promoted H3K27me3 demethylation and upregulation of KDM6B expression in $CD90^+$ stem cells. These effects were inhibited under diabetic conditions but were partially reversed by FPS-ZM1 treatment (Fig. 3e-f). In *vitro*, results demonstrated significant decreases in H3K27me3 expression under force, which was inhibited by AGEs but further reversed by FPS-ZM1 (Fig. 3g-h). In contrast, KDM6B saw an opposing trend, reflecting its regulatory role in histone modification (Fig. 3g-i).

#### AGEs impair force-induced osteogenic differentiation partially by inhibiting KDM6B

To further explore the relationship between KDM6B and osteogenesis, osteogenic markers were first analyzed under different conditions. In *vivo*, mechanical force significantly elevated Alp and Runx2 expression, an effect inhibited by the diabetic environment but ameliorated by FPS-ZM1 treatment (Fig. 4a-b). In *vitro*, mechanical force increased ALP and RUNX2 protein and mRNA levels in PDLSCs, while AGEs inhibited their expression. This inhibition was reversed by targeting the AGEs/RAGE pathway with FPS-ZM1 (Fig. 4c-d). Similar trends were observed in ALP activity assays (Fig. 4e). These findings suggest that AGEs impair force-induced osteogenic differentiation.

Further in *vitro* studies were conducted to investigate whether AGEs inhibit osteogenesis via KDM6B. A comparison of AGEs and GSK-J4, both individually and in combination, revealed no significant additive effects on ALP and RUNX2 mRNA and protein expression levels (Fig. 5a-b). ALPase activity and Alizarin red S staining results further supported these findings (Fig. 5c-d). Alizarin red S staining indicated that GSK-J4 inhibited the formation of fine mineralized nodules, unlike AGEs, suggesting distinct effects on osteogenesis and KDM6B inhibition (Fig. 5d). To further confirm the role of KDM6B, overexpression of KDM6B (OE-KDM6B) was used to rescue the inhibitory effect of AGEs on osteogenesis. OE-KDM6B significantly increased RUNX2 and ALP mRNA and protein levels in the presence of AGEs (Fig. 5e-f), with similar trends observed in ALPase activity and Alizarin red S staining (Fig. 5g-h).

#### AGEs inhibit the mechanical sensitivity of KDM6B by affecting the self-reinforcing loop between KDM6B and the wnt signalling pathway

Activation of the Wnt signalling pathways is crucial for regulating transcription factors during stem cell differentiation, encompassing the Wnt/β-catenin, Wnt/PCP, and $Wnt/Ca^{2+}$ pathways. GSEA and KEGG analyses revealed that mechanical force and KDM6B overexpression led to the activation of these pathways (Figs. 2f and 6a). Significant alterations were observed in upstream, midstream, and downstream components of the Wnt/β-catenin and $Wnt/Ca^{2+}$ pathways, leading to upregulation of TCF and NFATC transcription factor families (Fig. 6b-c). In *vivo* analysis showed that the diabetic microenvironment

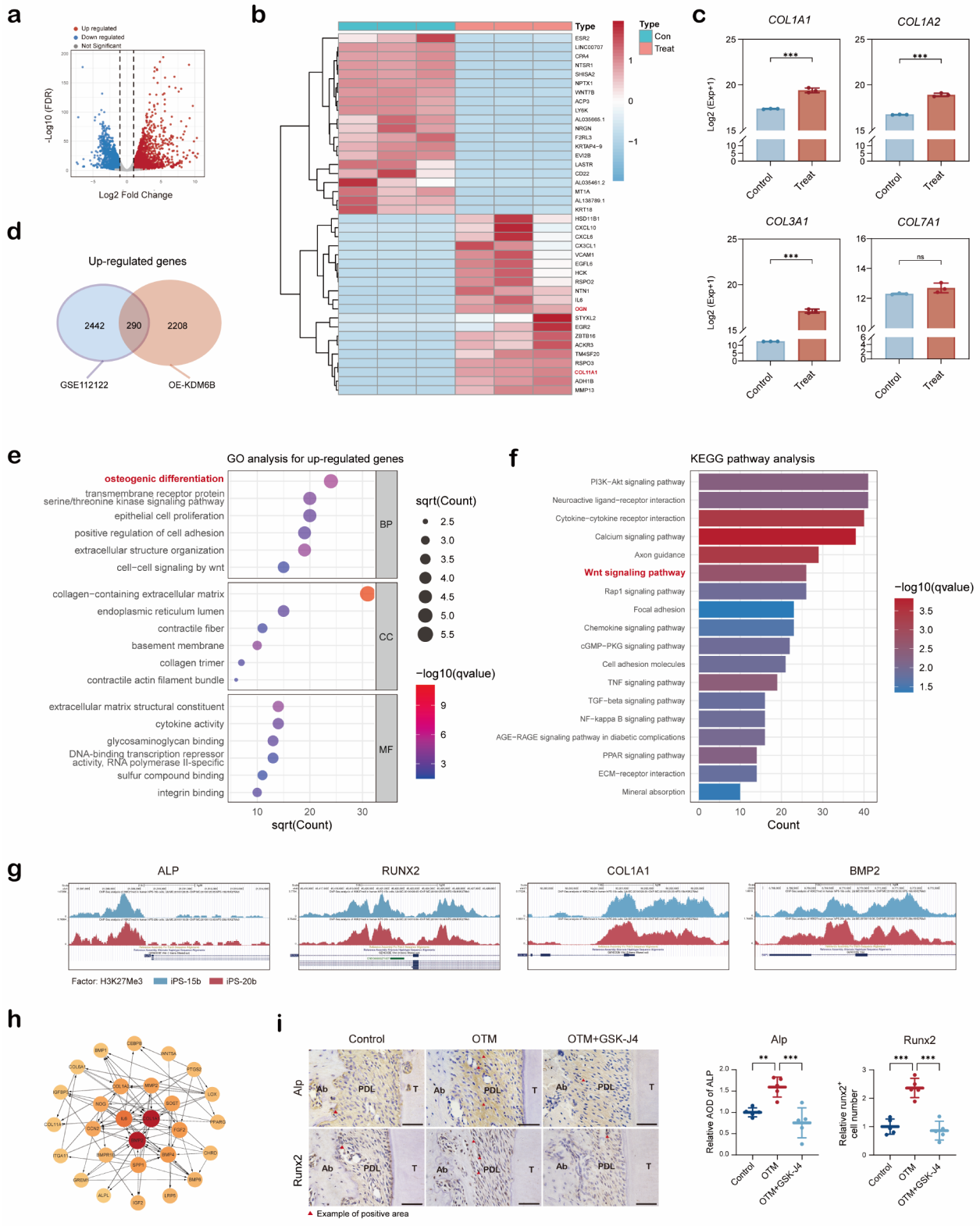


**Fig. 2** KDM6B broadly regulates the downstream transcriptome induced by mechanical stimulation. (**a**) Volcano plot of DEGs following OE-KDM6B treatment. (**b**) Heatmap of the top 20 upregulated and downregulated DEGs. (**c**) Expression differences in periodontal collagen-related genes. (**d**) Venn diagram showing common upregulated DEGs between the OE-KDM6B and GSE112122 datasets. (**e**) GO analysis of common DEGs, illustrating BP, CC, and MF terms. (**f**) KEGG pathway analysis of common DEGs. (**g**) ChIP-Seq analysis showing H3K27Me3 enrichment at transcription start sites and within gene bodies. (**h**) PPI network identifying an osteogenesis-related subnetwork. (**i**) IHC showing the effects of orthodontic force and GSK-J4 on the expression of osteogenesis-related markers (Alp and Runx2, $n = 5$). Data are presented as mean ± SD. Statistical significance: $^{*}P < 0.05$, $^{**}P < 0.01$, $^{***}P < 0.001$

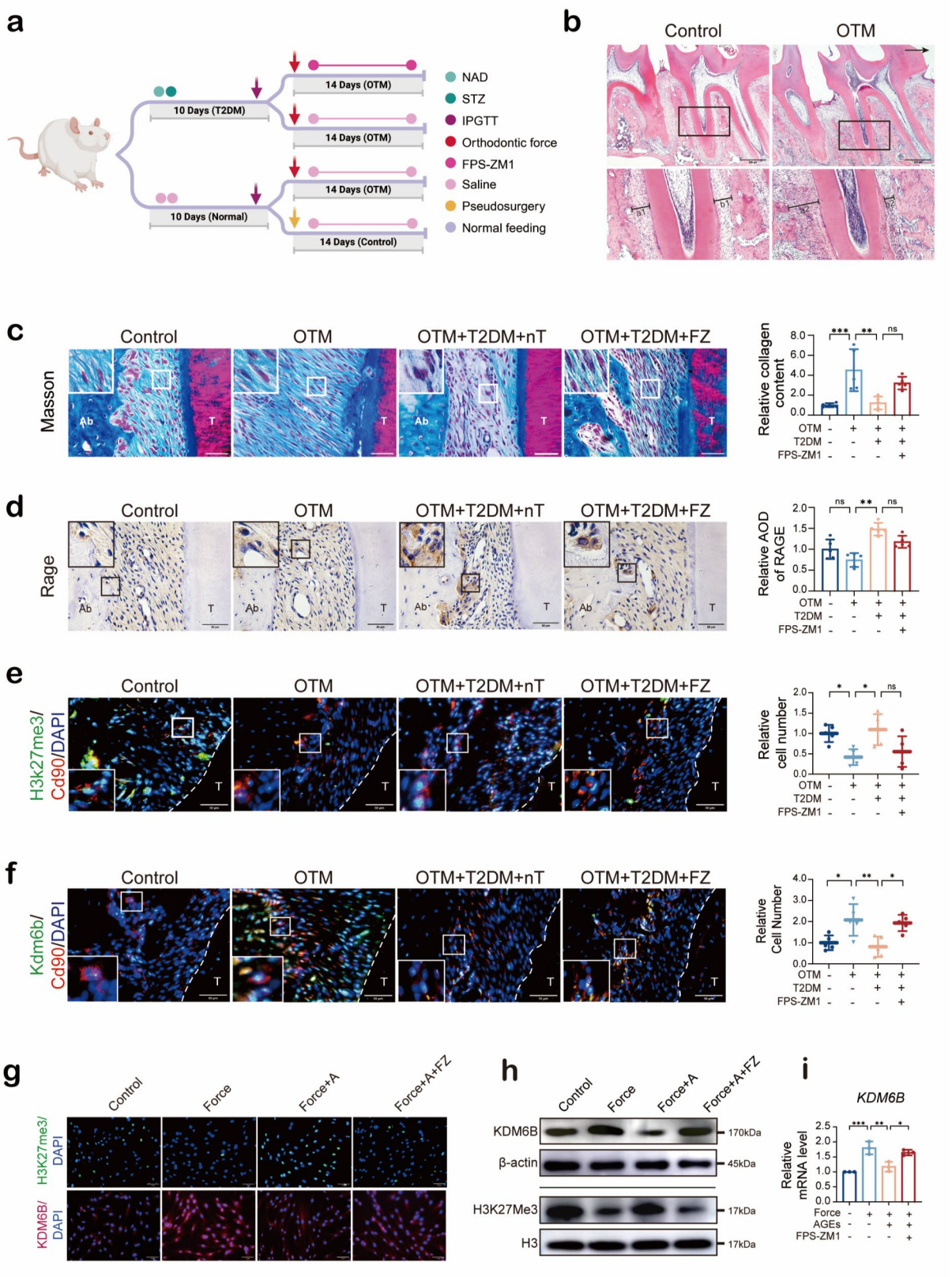


**Fig. 3** (See legend on next page.)

(See figure on previous page.)

**Fig. 3** AGEs inhibit mechanical force-induced KDM6B expression. (**a**) Schematic of the animal model created with BioRender.com. (**b**) Changes in periodontal ligament width after force application observed by HE staining (scale bar = 100 μm). (**c**) Collagen morphology and relavite content were assessed by Masson's trichrome staining (scale bar = 50 μm). (**d**) RAGE levels detected by IHC (scale bar = 50 μm). (**e**, **f**) Immunofluorescence of KDM6B and H3K27me3 in CD90-positive stem cells, with nuclei stained by DAPI (blue, scale bar = 50 μm). (**g**) Immunofluorescence of KDM6B and H3K27me3 in PDLSCs, with DAPI (blue) for nuclear staining (scale bar = 75 μm). (**h**) Western blot of KDM6B and H3K27me3 protein levels, with β-actin and H3 as loading controls, respectively; (**i**) The qRT-PCR for KDM6B mRNA using *ACTB* as reference gene. In *vivo* experiments: $n = 5$, in *vitro* experiments: $n = 3$. "FZ" indicates FPS-ZM1 treatment. "nT" means no treatment was administered. Data are presented as mean ± SD. Statistical significance: $^{*}P < 0.05$, $^{**}P < 0.01$, $^{***}P < 0.001$

inhibited Wnt pathway activation. Wnt2 and Wnt5A, ligands known to activate canonical and noncanonical pathways respectively, were upregulated by orthodontic force in the periodontal ligament, while their expression was suppressed in the diabetic microenvironment. This suppression was reversed by FPS-ZM1 treatment (Fig. 6d). Immunofluorescence co-labelling of Cd90 with β-catenin or Camk II revealed similar trends (Fig. 6e), indicating that AGEs inhibit the activation of Wnt signalling.

To further explore the relationship between KDM6B and Wnt signaling, overexpression of KDM6B (OE-KDM6B) significantly increased the levels of active β-catenin and p-CAMK II proteins (Fig. 6f). Immunofluorescence confirmed elevated β-catenin levels and nuclear translocation following KDM6B overexpression (Fig. 6g). Calcium ion detection assays revealed increased intracellular calcium levels after OE-KDM6B treatment, while KDM6B inhibition produced the opposite effect (Fig. 6h). These results suggest that KDM6B mediates the activation of both the Wnt/β-catenin and Wnt/$Ca^{2+}$ pathways. Motif analysis predicted that TCF7 and NFATC4 could bind to the transcription start site of KDM6B, promoting its transcription (Fig. 6i). To validate this, cells were treated with the Wnt pathway activator LiCl and inhibitor XAV-939. LiCl promoted KDM6B upregulation and H3K27Me3 demethylation, while XAV-939 suppressed both (Fig. 6j-k), indicating a positive feedback mechanism between KDM6B and Wnt signalling.

### Activation of the KDM6B/Wnt self-reinforcing loop improves AGEs-induced senescence and oxidative damage in PDLSCs

The primary causes of impaired osteogenic differentiation in stem cells are senescence and inflammation, with inflammatory ROS significantly contributing to cellular senescence. β-Galactosidase staining indicated that neither mechanical force nor KDM6B overexpression/inhibition directly induced senescence in PDLSCs (Fig. 7a). However, AGEs significantly induced senescence, which was partially reversed by OE-KDM6B (Fig. 7a). ROS detection revealed a similar trend, suggesting that AGEs disrupt cellular ROS repair mechanisms (Fig. 7b). Sequencing indicated upregulation of ROS damage repair genes, including *SOD2*, *NFE2L2*, *GPX4*, and *GPX7*, following KDM6B overexpression (Fig. 7c). ChIP-seq showed significant enrichment of H3K27me3 at the *SOD2* and *GPX7* loci (Fig. 7d). The qRT-PCR demonstrated that mechanical force and OE-KDM6B increased *SOD2* expression, while AGEs and GSK-J4 had the opposite effect (Fig. 7e). Immunofluorescence confirmed these results (Fig. 7f). Given the role of SOD2 in mitochondrial homeostasis, which is regulated through the Wnt/$Ca^{2+}$ pathway and TNTs, mechanical force was found to promote TNTs production, with KDM6B closely associated with TNTs regulatory factors (Figure S4). OE-KDM6B increased both TNTs and SOD2 levels, while the Wnt/$Ca^{2+}$ pathway inhibitor KN-93 significantly reduced TNTs and SOD2 expression (Fig. 7g). The qRT-PCR results showed a similar trend, with the increase in Wnt/β-catenin also promoting SOD2 expression, while the opposite effect was observed when it was inhibited (Fig. 7h).

## Discussion

This study revealed that orthodontic force-induced KDM6B played a critical role in regulating various biological functions and signalling pathways associated with osteogenesis. AGEs impaired the osteogenic differentiation capacity of PDLSCs by modulating KDM6B expression. Notably, the findings indicated that KDM6B and the Wnt signalling pathway formed a self-reinforcing loop, which may have served as a potential mechanism by which AGEs affected KDM6B. Furthermore, modulation of the KDM6B/Wnt loop alleviated AGEs-induced oxidative stress and cellular senescence. The overall mechanism proposed in this study is illustrated in Fig. 8.

Given that alveolar bone remodelling occurs during the early phase of OTM [28], the force application timeframe in our study was specifically designed to replicate this initial stage. Our findings further support that cyclic tension stress (24 h, 10%, 0.5 Hz) effectively promotes osteoblastic differentiation and proliferation, consistent with the characteristics of early OTM [19, 29]. While the role of appropriate orthodontic forces in promoting osteogenesis has been extensively documented, it remains underexplored in some areas. Scientists have focused on epigenetic changes during stem cell differentiation and have uncovered their significant implications, yet further efforts are still needed in the area of histone modifications [30]. Analysis of the GEO dataset and experimental validation revealed the mechanosensitivity of KDM6B. Similarly, research by Jin et al. [16] indicated that mechanical force could alter the function of KDM6B

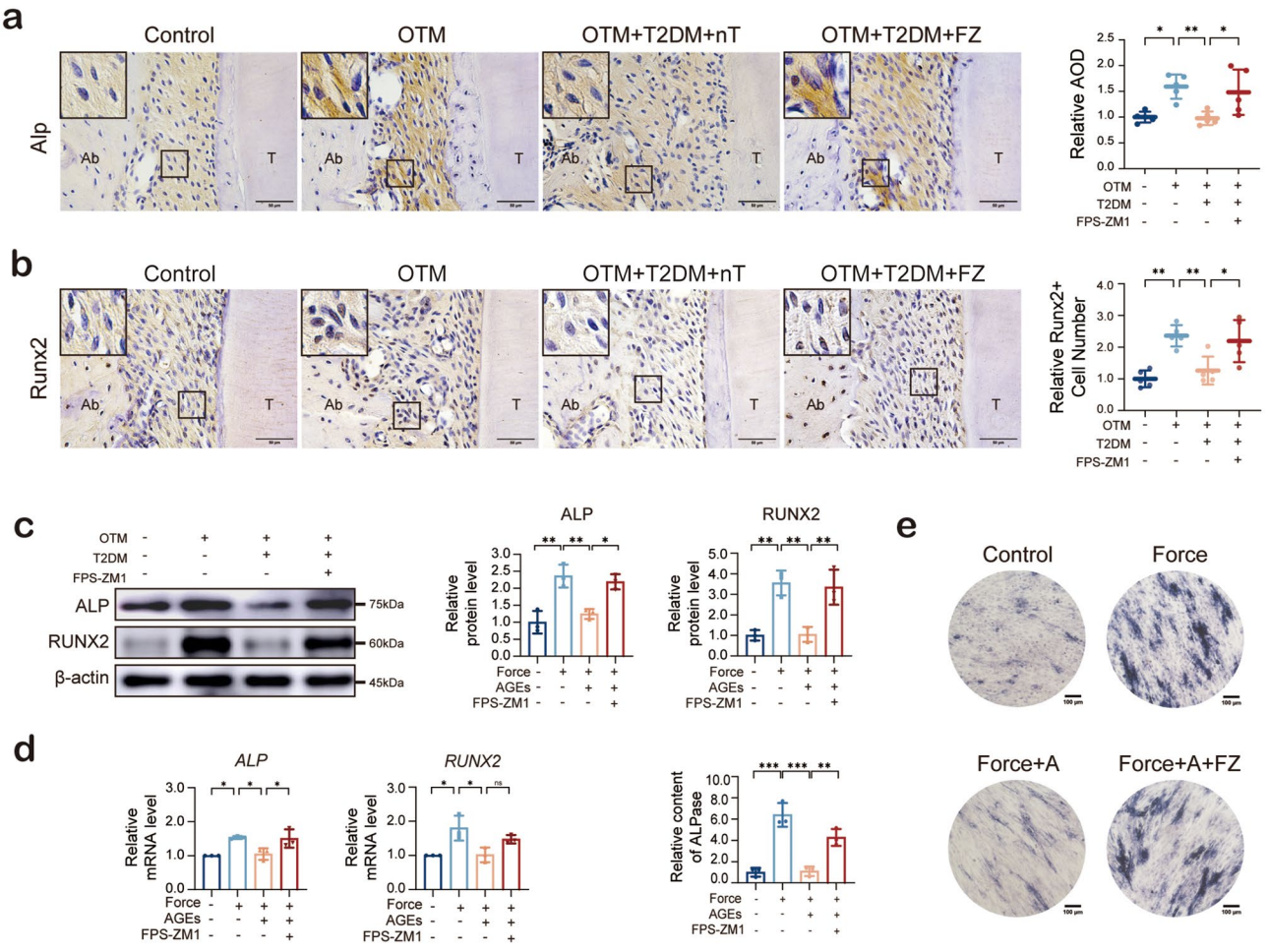


**Fig. 4** AGEs inhibit mechanical force-induced osteogenesis. (**a**, **b**) IHC show the levels of Alp and Runx2 in tissues ($n=5$). (**c**) Western blot analysis of ALP and RUNX2 protein levels in PDLSCs, with β-actin as a loading control ($n=3$). (**d**) qRT-PCR analysis of *ALP* and *RUNX2* mRNA levels in PDLSCs, using *ACTB* as a reference gene ($n=3$). (**e**) ALPase staining to detect ALP activity ($n=3$). Data are presented as mean ± SD. Statistical significance: $^{*}P<0.05$, $^{**}P<0.01$, $^{***}P<0.001$

in chondrocytes, resulting in changes in inflammation. Moreover, the downregulation of EZH2 by mechanical forces also suggested that the expression and function of KDM6B might have been altered [31].

The role of KDM6B has garnered significant attention from researchers. This gene could promote odontogenic differentiation of dental pulp-derived stem cells by removing H3K27Me3 from osteogenic markers [32], which was consistent with our findings. Inhibiting KDM6B reduced type I collagen content and delayed angiogenesis, leading to decreased cell viability and adhesion [33]. Our study also highlighted KDM6B's regulatory role in collagen synthesis, as OE-KDM6B upregulated this process. Additionally, the absence of mineralized nodules following KDM6B inhibition indicated early-stage defects in matrix synthesis and secretion. K-H Chiu et al. [34] reported that cyclic stretching enhanced the directional alignment of collagen fibres and increased the proliferation and migration of periodontal ligament cells. This mechanical stimulation also promoted extensive extracellular matrix remodelling and glycosaminoglycan synthesis [34]. However, the detrimental effects of AGEs on collagen and the extracellular matrix cannot be overlooked [35]. In this study, AGEs inhibited both collagen synthesis and reorganization while also inducing collagen ageing and degradation during OTM. Given that AGEs suppressed KDM6B's mechanosensitivity, it is plausible that AGEs impaired collagen synthesis during force-induced osteogenic differentiation by inhibiting KDM6B.

Notably, all identified changes in histone marks and their effects are reversible, and most regulatory signals diminish rapidly in the absence of a robust self-reinforcing loop to sustain chromatin state memory [36]. Recent work by Han S et al. [37] suggested that feedback loops between mechanotransduction and histone modifications may serve as potential therapeutic targets in clinical applications. Furthermore, other studies have demonstrated significant upregulation of the Wnt/β-catenin and

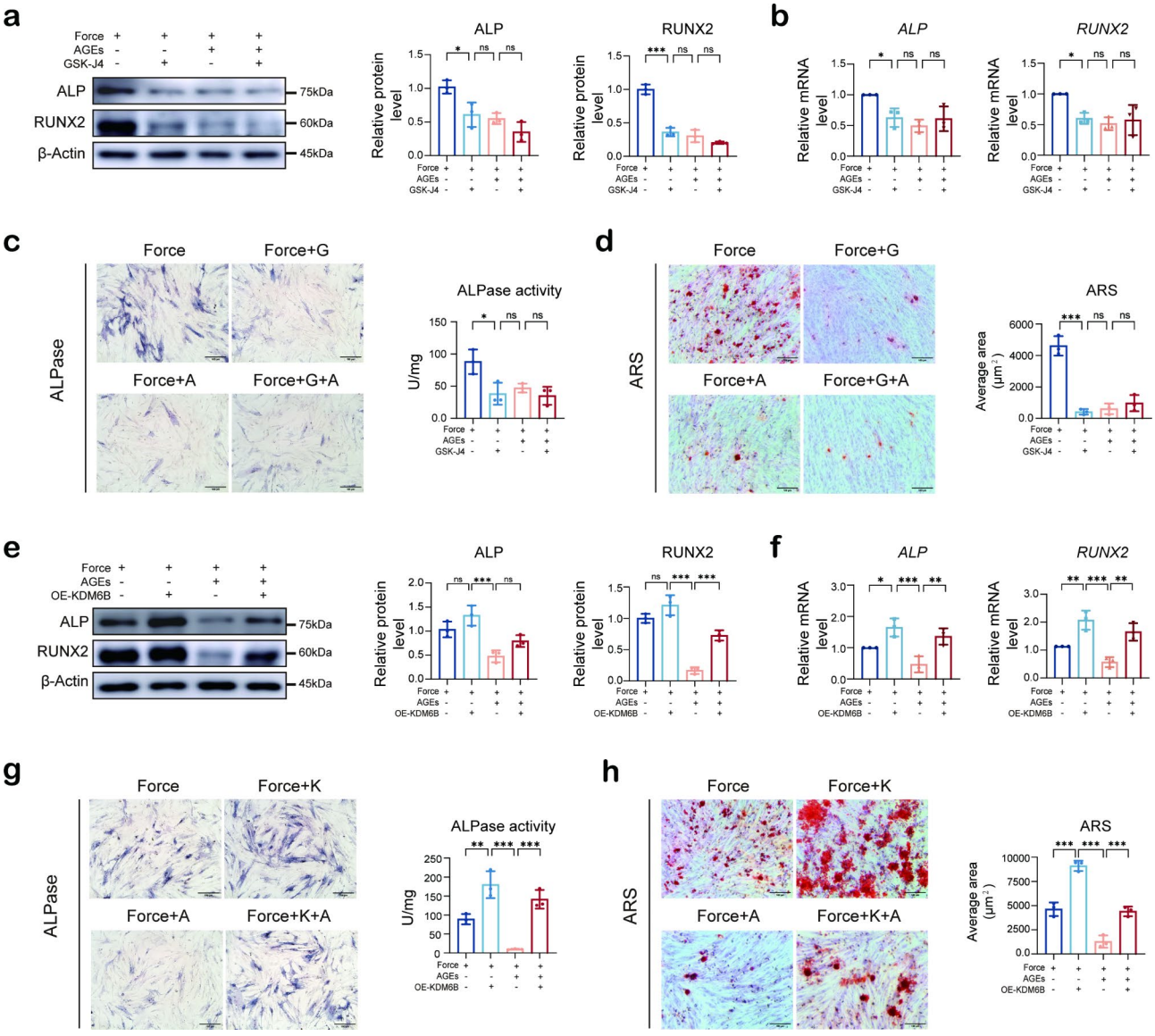


**Fig. 5** AGEs influence osteogenic differentiation partially through KDM6B. (**a**, **e**) Western blot analysis of ALP and RUNX2 protein levels in PDLSCs, with β-actin as a loading control ($n=3$). (**b**, **f**) qRT-PCR analysis of *ALP* and *RUNX2* mRNA levels in PDLSCs, using *ACTB* as a reference gene ($n=3$). (**c**, **g**) ALPase staining to detect ALP activity and early osteogenic differentiation potential ($n=3$). (**d**, **h**) ARS staining to detect late osteogenic differentiation potential ($n=3$). "G" represents GSK-J4 treatment, "A" represents AGEs treatment, and "K" represents KDM6B overexpression. Data are presented as mean ± SD. Statistical significance: $^{*}P<0.05$, $^{**}P<0.01$, $^{***}P<0.001$

Wnt/$Ca^{2+}$ pathways during OTM [38], which aligns with our findings. Li et al. [39] reported that prolonged Wnt signalling activation disrupts the abnormal distribution of H3K27Me3. CAMK II, a key mediator of the Wnt/$Ca^{2+}$ pathway, has also been shown to reduce SOX2-associated H3K27Me3, thereby enhancing gene function upon activation [40]. The present study consistently indicated that activation of both the canonical and noncanonical Wnt pathways could positively influence KDM6B. Notably, we revealed extensive activation of the Wnt pathway following OE-KDM6B, consistent with the findings of Ohtani et al. [41], who elucidated the role of KDM6B in diminishing H3K27Me3 while facilitating β-catenin recruitment. Additionally, prior research demonstrated that human embryonic stem cells could promote mesodermal differentiation by reducing H3K27Me3 occupancy at mesodermal gene promoters and activating the Wnt/β-catenin signalling pathway [42]. Based on these observations, we propose that the Wnt pathway forms a self-reinforcing loop with KDM6B, although further experimental validation is needed to clarify the specific transcriptional sites where KDM6B interacts with the TCF/LEF and NFAC families.

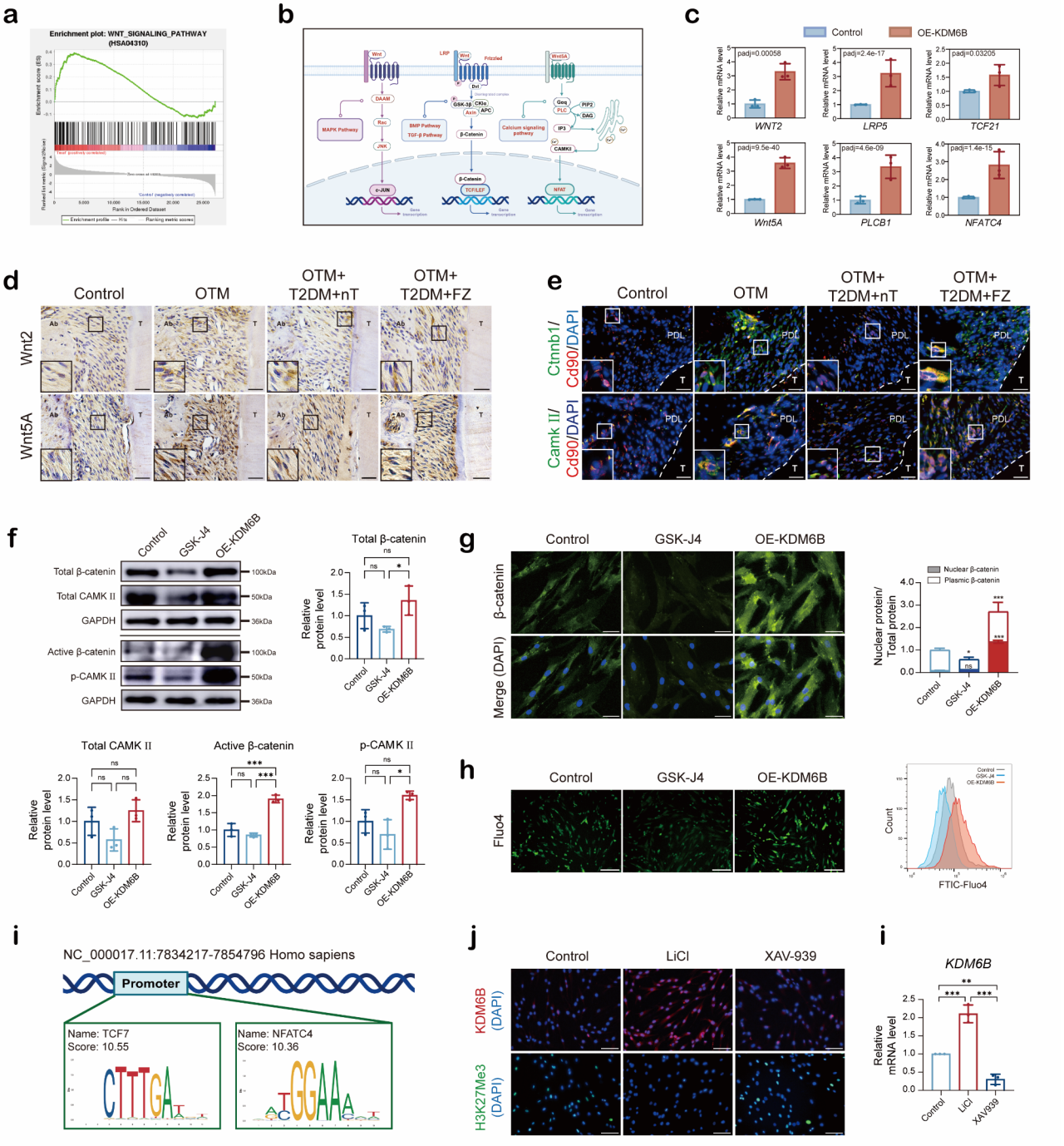


**Fig. 6** AGEs impair Wnt signalling pathways. (**a**) GSEA showed activation of the Wnt pathway in the OE-KDM6B group. (**b**) Schematic diagram displaying the three components of the Wnt pathway, with DEGs regulated by KDM6B and mechanical force marked in red, created with BioRender.com. (**c**) Box plots showing specific DEGs related to the Wnt/β-catenin and Wnt/$Ca^{2+}$ pathways following OE-KDM6B. (**d**) IHC revealed changes in the expression of Wnt2 and Wnt5A in the periodontal ligament (scale bar = 50 μm). (**e**) Immunofluorescence showing changes in the expression of β-catenin and CAMK II in CD90-positive cells (scale bar = 50 μm). (**f**) Western blot analysis of total β-catenin, active β-catenin, total CAMK II, and p-CAMK II expression levels, with GAPDH as a reference ($n = 3$). (**g**) Immunofluorescence analysis of relative β-catenin expression in the nucleus and cytoplasm (scale bar = 50 μm). (**h**) Intracellular $Ca^{2+}$ levels assessed using Fluo4-AM staining and detected by flow cytometry and fluorescence microscopy (scale bar = 50 μm). (**i**) Motif analysis of the transcription start region of the KDM6B gene. (**j**) Immunofluorescence analysis of KDM6B and H3K27Me3 expressions and the number of positively expressing cells (scale bar = 75 μm). (**k**) mRNA levels of *KDM6B* assessed by qRT-PCR, with *GAPDH* as a reference gene ($n = 3$). "nT" represents no treatment, and "FZ" represents FPS-ZM1 treatment. Data are presented as mean ± SD. Statistical significance: $^{*}P < 0.05$, $^{**}P < 0.01$, $^{***}P < 0.001$

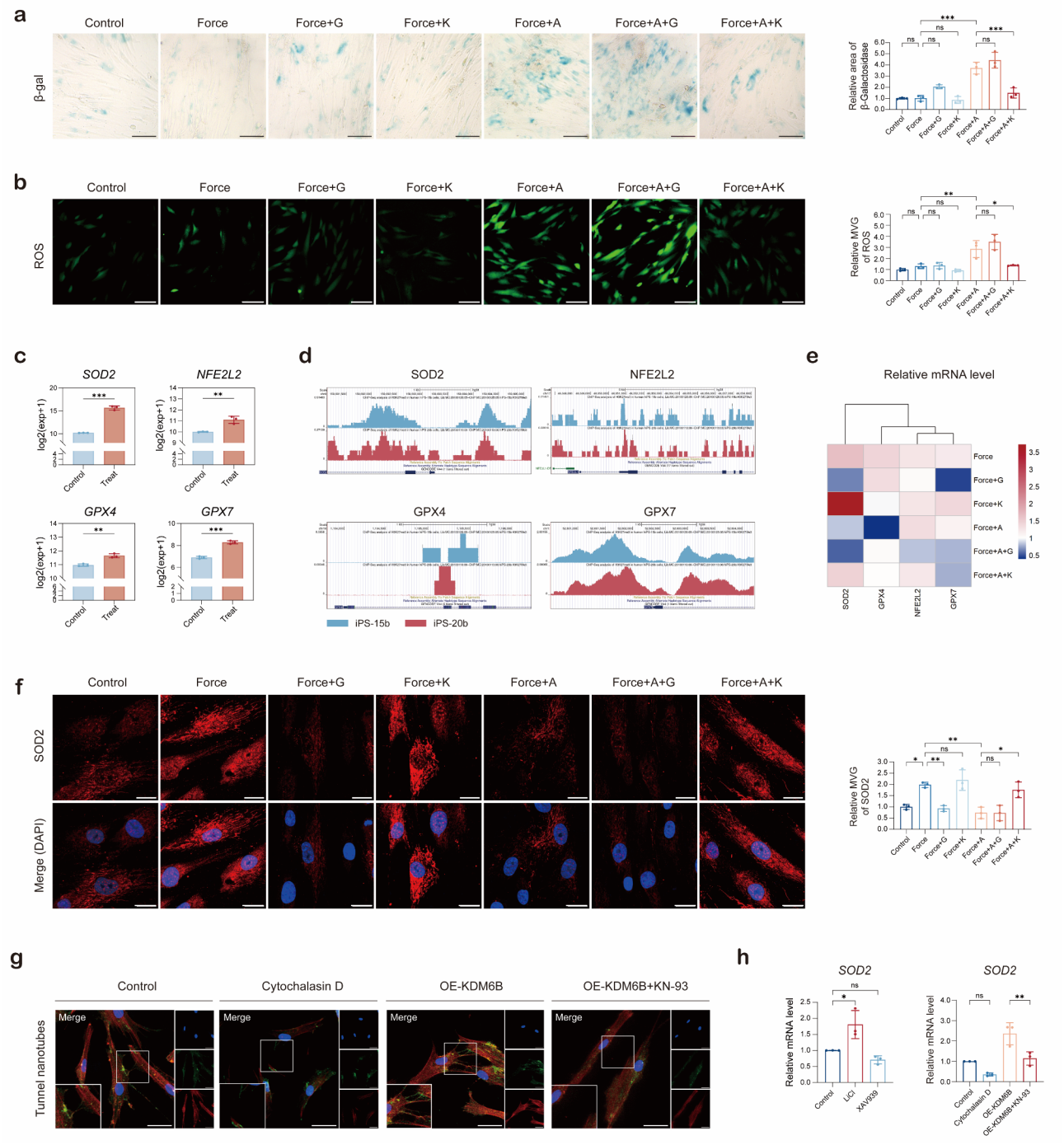


**Fig. 7** AGEs influence oxidative stress and stem cell ageing through the KDM6B/Wnt/SOD2 pathway. (**a**) β-Galactosidase assay detecting early ageing (scale bar = 50 μm, $n = 3$). (**b**) Intracellular ROS levels were measured using a ROS assay kit (scale bar = 50 μm, $n = 3$). (**c**) Expression differences of oxidative stress-related genes (SOD2, NFE2L2, GPX4, GPX7). (**d**) ChIP-seq showing H3K27me3 enrichment at the transcription start sites and regions of the SOD2, NFE2L2, GPX4, and GPX7 genes. (**e**) Heatmap showing the mRNA expression levels of SOD2, NFE2L2, GPX4, and GPX7 across different groups using qRT-PCR. (**f**) Confocal microscopy demonstrated the localization and expression of SOD2. (**g**) Confocal microscopy showing the colocalization of TNT and SOD2. DAPI (blue), SOD2 (green), and F-actin (red). (**h**) qRT-PCR analysis of *SOD2* mRNA levels in different groups. Statistical analyses were performed with $n = 3$. "A" represents AGEs, "G" represents GSK-J4, and "K" represents OE-KDM6B. Data are presented as mean ± SD. Statistical significance: $^{*}P < 0.05$, $^{**}P < 0.01$, $^{***}P < 0.001$

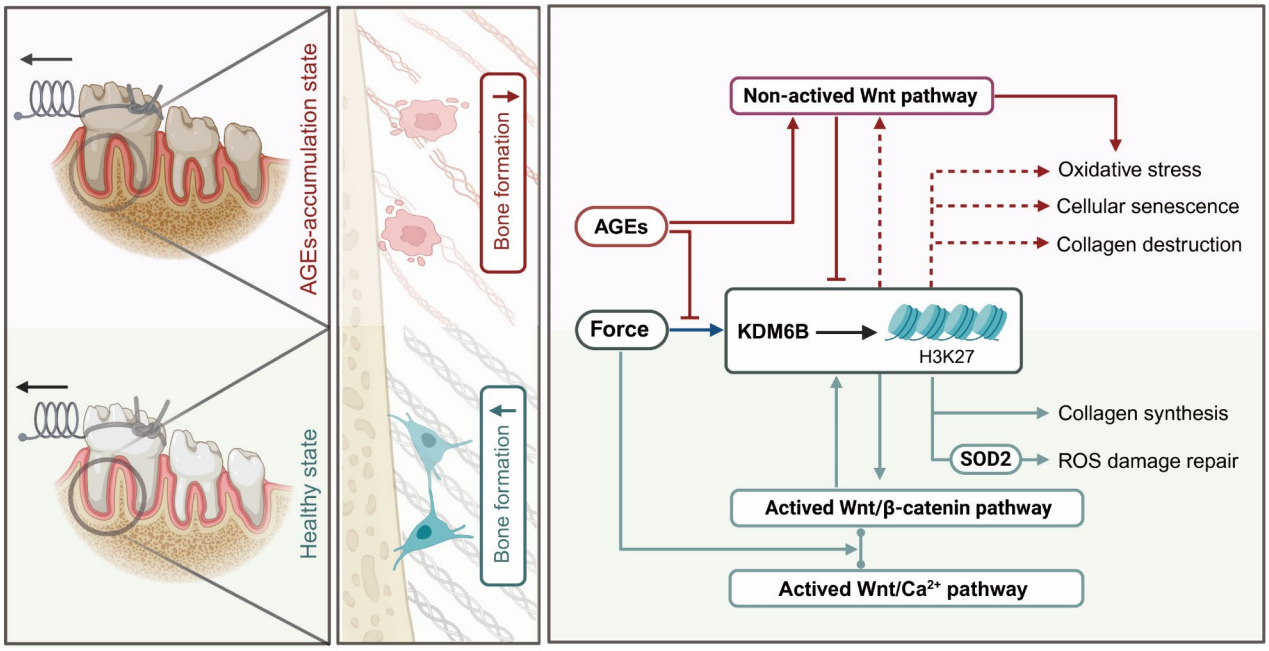


**Fig. 8** Schematic of AGEs regulation in the diabetic microenvironment. The diagram illustrates how AGEs regulate the antioxidant capacity of PDLSCs through the KDM6B/Wnt/SOD2 pathway, promoting stem cell senescence and inhibiting osteogenic differentiation. The figure was created with BioRender.com

The mechanisms by which AGEs impair the functionality of KDM6B are likely complex. First, AGEs may inhibit KDM6B by suppressing the KDM6B/Wnt loop via specific mechanisms, including Wnt glycosylation and β-catenin phosphorylation [43, 44]. However, the current research [43] revealed that Wnt5A was not significantly downregulated in T2DM patients, suggesting that inhibition of the noncanonical Wnt pathway may be attributed to the loss of function of Wnt5A caused by glycosylation. Moreover, the activation of the AGE/RAGE pathway resulting in ROS buildup may further promote the nonenzymatic glycation of proteinases [45], thereby leading to the inactivation of KDM6B. Previous studies have indicated that the Wnt pathway is involved in regulating DNA damage repair [46], so we focused mainly on KDM6B-associated DNA repair genes. These genes included SOD2, FOXO3, NFE2L2, and GPX4. Compared to other SOD isoenzymes, SOD2 is specifically located in the mitochondrial matrix and acts as the first line of defense in regulating ROS levels [47]. In certain inflammatory environments, SOD2 is upregulated as a self-repair mechanism in the body. Notably, the role of histone-modifying enzymes in regulating SOD2 has also attracted increased amounts of attention from scientists [48]. In this study, AGEs impaired the function of SOD2 by inhibiting the KDM6B/Wnt loop, thereby damaging the self-repair mechanism, which is likely the cause of the cascade amplification of ROS.

Inhibition of the KDM6B/Wnt/SOD2 pathway ultimately results in stem cell senescence. Although studies on the relationship between KDM6B and ageing are contradictory, the findings are complex. On the one hand, senescent cells exhibit widespread heterochromatinization and transcriptional repression driven by H3K27Me3 [49], suggesting an impediment to KDM6B function. On the other hand, some research has shown that KDM6B upregulates factors such as p16 and the senescence-associated secretory phenotype, which are linked to cell cycle arrest and ageing [50]. The present study further supported the former viewpoint.

Furthermore, the antioxidant capacity of cells is also related to intercellular interactions [51]. The formation of TNTs was the result of the rearrangement of actin filaments [24]. Healthy cells can provide functional mitochondria to damaged cells through TNTs, which serve as an efficient mechanism, enabling individual cells to maintain redox and metabolic homeostasis in a supercellular system [52]. The TNFAIP2/M-sec pathway is the key regulatory system for TNT formation [53]. The present study revealed that KDM6B regulated TNFAIP2 during the process of increased adhesion, which further demonstrated that orthodontic force promotes communication between stem cells in the form of TNTs. However, the maintenance of this process also requires the self-stabilizing effect of cells. Vargas et al. reported that Wnt/$Ca^{2+}$ pathway activation promoted TNT stability [25]. We also observed a decrease in the number of TNTs

after inhibition of the Wnt/$Ca^{2+}$ pathway; therefore, we hypothesized that AGEs may affect TNTs formation between PDLSCs via the KDM6B/Wnt/$Ca^{2+}$ pathway and subsequently influence the cellular oxidative balance. Similarly, other researchers have concluded that AGEs cannot change the expression of TNFAIP2 [53]. However, they also reported that AGEs still promoted TNT formation in podocytes. This effect may be related to the duration and concentration of AGE exposure. Whether PDLSCs can maintain cellular self-rescue states such as those of TNTs in the presence of AGEs requires further in-depth investigation.

The present study utilized animal models to simulate clinical conditions. Diverging from the conventional single-dose streptozotocin injection used to create a diabetic orthodontic model [54, 55], a Nicotinamide/Streptozotocin approach was employed to construct the T2DM animal model. This model more accurately represents the clinical characteristics of T2DM patients, likely diminishing the impact of high-fat diets, obesity, and age-related changes on orthodontic tooth movement [21]. Additionally, FPS-ZM1, a newly identified multimodal RAGE-specific inhibitor, exhibits minimal cytotoxicity and effectively blocks the AGEs/RAGE signalling pathway [56, 57]. Results demonstrated a significant enhancement in the osteogenic capability of periodontal ligament stem cells in the OTM+T2DM-FZ group compared to the OTM+T2DM-noTreat group, aligning with previous findings that RAGE-blocking can ameliorate diabetic osteoporosis [58]. Although the direct injection of Methylglyoxal (MG) has been explored to study the role of AGEs [56], this exogenous method is unsuitable for this research due to its inability to prove the accumulative effect of AGEs in periodontal tissues. Considering the established effects of AGEs on osteogenic differentiation and the role of FPS-ZM1 [59, 60], we opted not to include additional positive control groups to reduce statistical and ethical burdens. Thus, the modelling approach employed in this experiment is deemed more physiologically relevant, extending current methodologies for modelling T2DM in the context of OTM.

However, this study has limitations. The T2DM models did not explore KDM6B overexpression's therapeutic potential, and focusing solely on one histone modification may be too narrow. Additionally, we did not examine H3K27Me3 enrichment in various genes using Chip-seq. Future studies should systematically evaluate the diabetic microenvironment's effects on various histone modifications. Moreover, the impact of different types and severities of diabetes on orthodontic treatment, as well as corresponding management strategies, needs further refinement to improve clinical practice guidelines. Our findings suggest that combining epigenetic or Wnt pathway modulators with RAGE blockers could enhance orthodontic treatment outcomes in diabetic patients. This approach offers a more personalized treatment strategy, potentially improving patient-specific responses and overall therapeutic efficacy.

## Conclusions

In conclusion, our research revealed that AGEs downregulate the expression and function of KDM6B under mechanical stress, impeding H3K27Me3 clearance in PDLSCs. This diminished osteogenic gene expression and disrupted the KDM6B/Wnt self-reinforcing loop. Dysregulation of the loop affected SOD2 and TNTs, thereby leading to ROS accumulation and stem cell ageing. We proposed a novel mechanism involving the KDM6B/Wnt/SOD2 pathway in PDLSCs under a mechanical microenvironment.

## Supplementary Information

The online version contains supplementary material available at https://doi.org/10.1186/s13287-024-04058-8.

Supplementary Material 1

Supplementary Material 2

Supplementary Material 3

Supplementary Material 4

Supplementary Material 5

Supplementary Material 6

Supplementary Material 7

### Acknowledgements

We thank Dr. Jianming Zeng (University of Macau) and all the members of his bioinformatics team, Biotrainee, for generously sharing their experiences and codes. We thank the team of Manokawinchoke J from Chulalongkorn University for providing the GSE112122 sequencing data in the GEO database.

### Author contributions

Q. Y. contributed to the conception, design, data acquisition, analysis, interpretation, and drafting of the manuscript. Y. J. and C. S. contributed to the study conception and data acquisition, and they critically revised the manuscript. Y. Z. and R. G. contributed to the interpretation and critically revised the manuscript. H. L. contributed to the analysis and critically revised the manuscript. H. L., J. G. and M. L. contributed to the conception of the study and critically revised the manuscript. All authors gave final approval and agreed to be accountable for all aspects of the work. The authors declare that artificial intelligence is not used in this study.

### Funding

This study was partially supported by the TaiShan Scholars of Shandong Province (No. tstp20221160) to Minqi Li, the National Natural Science Foundation of China (No. 82370999), the Horizontal Project of Shandong University (No. 1350022008) to Jie Guo, the Construction Engineering Special Fund of Taishan Young Scholars of Shandong Province (No. tsqn202103177) and the Natural Science Foundation of Shandong Province (No. ZR202210210042) to Hongrui Liu.

### Data availability

Our RNA-seq data has been uploaded to the GEO database (https://www.ncbi.nlm.nih.gov/geo/) with the accession number GSE264552. Other underlying research materials can be obtained from the corresponding authors. The remaining data in the manuscript can be found in the supplementary files. Supplementary File 6 contains information on the supplementary figures.

## Declarations

### Ethical approval

This study involves a human research project titled "Mechanism of Orthodontic Force-Induced Osteogenic Differentiation of PDLSCs Affected by the Diabetic Microenvironment via KDM6B". It has been reviewed and approved by the Ethics Committee of the Hospital of Stomatology, Shandong University. The ethics approval number is NO. 20231115, and the approval date is November 30, 2023. Additionally, this research includes an animal experiment ethics project entitled "Mechanism of Orthodontic Force-Induced Osteogenic Differentiation of PDLSCs Influenced by the Diabetic Microenvironment through KDM6B". It has received approval from the Ethics Committee of the Hospital of Stomatology, Shandong University, with the ethics approval number NO. 20231116 granted on November 30, 2023.

### Consent to participate

The acquisition of human PDLSCs involved in this study was obtained with informed consent from the patients, and written informed consent was obtained from the patients or their guardians for participation and the use of samples.

### Consent to publish

The authors affirm that human research participants provided informed consent for the publication of the images related to PDLSCs.

### Conflict of interests

The authors declare no potential conflicts of interest concerning the research, authorship, or publication of this article.

### Author details

[1]Department of Bone Metabolism, School and Hospital of Stomatology, Cheeloo College of Medicine, Shandong Key Laboratory of Oral Tissue Regeneration & Shandong Engineering Research Center of Dental Materials and Oral Tissue Regeneration & Shandong Provincial Clinical Research Center for Oral Diseases, Shandong University, No.44-1 Wenhua Road West, Jinan, Shandong 250012, China
[2]Center of Osteoporosis and Bone Mineral Research, Shandong University, Jinan, Shandong, China
[3]Department of Orthodontics, School and Hospital of Stomatology, Cheeloo College of Medicine, Shandong University, Jinan, Shandong, China
[4]Department of Periodontology, School and Hospital of Stomatology, Cheeloo College of Medicine, Shandong University, Jinan, Shandong, China
[5]School of Clinical Medicine, Jining Medical University, Jinan, Shandong, China

Received: 11 June 2024 / Accepted: 10 November 2024
Published online: 15 November 2024

### References

1. Marklund M, Braem MJA, Verbraecken J. Update on oral appliance therapy. Eur Respir Rev off J Eur Respir Soc. 2019;28:190083.
2. Xu K, Zhang L, Yu N, Ren Z, Wang T, Zhang Y, et al. Effects of advanced glycation end products (AGEs) on the differentiation potential of primary stem cells: a systematic review. Stem Cell Res Ther. 2023;14:74.
3. Wang K, Xu C, Xie X, Jing Y, Chen PJ, Yadav S, et al. Axin2 + PDL cells directly contribute to new alveolar bone formation in response to Orthodontic Tension Force. J Dent Res. 2022;101:695–703.
4. Olson LC, Nguyen T, Sabalewski EL, Puetzer JL, Schwartz Z, McClure MJ. S100b treatment overcomes RAGE signaling deficits in myoblasts on advanced glycation end-product cross-linked collagen and promotes myogenic differentiation. Am J Physiol Cell Physiol. 2024;326:C1080–93.
5. He W, Fu Y, Yao S, Huang L. Programmed cell death of periodontal ligament cells. J Cell Physiol. 2023;238:1768–87.
6. Bjornstad P, Chao LC, Cree-Green M, Dart AB, King M, Looker HC, et al. Youth-onset type 2 diabetes mellitus: an urgent challenge. Nat Rev Nephrol. 2023;19:168–84.
7. International Hypoglycaemia Study Group. Hypoglycaemia, cardiovascular disease, and mortality in diabetes: epidemiology, pathogenesis, and management. Lancet Diabetes Endocrinol. 2019;7:385–96.
8. Yamagishi S-I, Nakamura N, Matsui T. Glycation and cardiovascular disease in diabetes: a perspective on the concept of metabolic memory. J Diabetes. 2017;9:141–8.
9. Wang N, Zhang C, Oxidative Stress. A culprit in the Progression of Diabetic kidney disease. Antioxid Basel Switz. 2024;13:455.
10. Wang B, Vashishth D. Advanced glycation and glycoxidation end products (AGEs/AGOEs) in bone. Bone. 2023;176:116880.
11. Kamran MA. Salivary and crevicular fluid proinflammatory cytokines and advanced glycation end products in patients with different glycemic levels undergoing fixed orthodontic treatment. Angle Orthod. 2024;94:233–9.
12. Rehman S, Aatif M, Rafi Z, Khan MY, Shahab U, Ahmad S, et al. Effect of nonenzymatic glycosylation in the epigenetics of cancer. Semin Cancer Biol. 2022;83:543–55.
13. Koestler SA, Ball ML, Muresan L, Dinakaran V, White R. Transcriptionally active chromatin loops contain both active and inactive histone modifications that exhibit exclusivity at the level of nucleosome clusters. Epigenetics Chromatin. 2024;17:8.
14. Zhou Y, Zheng L, Li F, Wan M, Fan Y, Zhou X, et al. Bivalent histone codes on WNT5A during odontogenic differentiation. J Dent Res. 2018;97:99–107.
15. Liu Z, Lee H-L, Suh JS, Deng P, Lee C-R, Bezouglaia O, et al. The ERα/KDM6B regulatory axis modulates osteogenic differentiation in human mesenchymal stem cells. Bone Res. 2022;10:3.
16. Jin Y, Liu Z, Li Z, Li H, Zhu C, Li R, et al. Histone demethylase JMJD3 downregulation protects against aberrant force-induced osteoarthritis through epigenetic control of NR4A1. Int J Oral Sci. 2022;14:34.
17. Nakka K, Hachmer S, Mokhtari Z, Kovac R, Bandukwala H, Bernard C, et al. JMJD3 activated hyaluronan synthesis drives muscle regeneration in an inflammatory environment. Science. 2022;377:666–9.
18. Arifin WN, Zahiruddin WM. Sample size calculation in Animal studies using resource equation Approach. Malays J Med Sci MJMS. 2017;24:101–5.
19. Wang J, Yang H, Ma X, Liu J, Li L, Chen L, et al. LRP6/filamentous-actin signaling facilitates osteogenic commitment in mechanically induced periodontal ligament stem cells. Cell Mol Biol Lett. 2023;28:7.
20. Sayed HM, Awaad AS, Abdel Rahman FE-ZS, Al-Dossari M, Abd El-Gawaad NS, Ahmed OM. Combinatory Effect and modes of Action of Chrysin and Bone Marrow-derived mesenchymal stem cells on Streptozotocin/Nicotinamide-Induced Diabetic rats. Pharm Basel Switz. 2022;16:34.
21. Yan L-J. The Nicotinamide/Streptozotocin rodent model of type 2 diabetes: renal pathophysiology and Redox Imbalance features. Biomolecules. 2022;12:1225.
22. Meng L, Yang P, Zhang W, Zhang X, Rong X, Liu H, et al. Brain-derived neurotrophic factor promotes orthodontic tooth movement by alleviating periodontal ligament stem cell senescence. Cell Signal. 2023;108:110724.
23. Gong X, Sun S, Yang Y, Huang X, Gao X, Jin A, et al. Osteoblastic STAT3 is crucial for Orthodontic Force Driving alveolar bone remodeling and tooth Movement. J Bone Min Res off J Am Soc Bone Min Res. 2023;38:214–27.
24. Cordero Cervantes D, Zurzolo C. Peering into tunneling nanotubes—the path forward. EMBO J. 2021;40:e105789.
25. Vargas JY, Loria F, Wu Y-J, Córdova G, Nonaka T, Bellow S, et al. The Wnt/Ca2 + pathway is involved in interneuronal communication mediated by tunneling nanotubes. EMBO J. 2019;38:e101230.
26. Komori T. Whole aspect of Runx2 functions in skeletal development. Int J Mol Sci. 2022;23:5776.
27. Ae L, Jg C, Sh S, Qz PH, Ad Z. DPSC-Derived Extracellular vesicles promote rat Jawbone Regeneration. J Dent Res. 2023;102(3):313–21.
28. Huelter-Hassler D, Tomakidi P, Steinberg T, Jung BA. Orthodontic strain affects the Hippo-pathway effector YAP concomitant with proliferation in human periodontal ligament fibroblasts. Eur J Orthod. 2017;39:251–7.
29. Krishnan V, Davidovitch Z. On a path to unfolding the biological mechanisms of orthodontic tooth movement. J Dent Res. 2009;88:597–608.
30. Gu T, Guo R, Fang Y, Xiao Y, Chen L, Li N, et al. METTL3-mediated pre-miR-665/DLX3 m6A methylation facilitates the committed differentiation of stem cells from apical papilla. Exp Mol Med. 2024;56:1426–38.
31. Li Q, Sun X, Tang Y, Qu Y, Zhou Y, Zhang Y. EZH2 reduction is an essential mechanoresponse for the maintenance of super-enhancer polarization against compressive stress in human periodontal ligament stem cells. Cell Death Dis. 2020;11:757.
32. Ding Y, Yao Y, Gong X, Zhuo Q, Chen J, Tian M, et al. JMJD3: a critical epigenetic regulator in stem cell fate. Cell Commun Signal CCS. 2021;19:72.

33. Qi L, Lu Y, Wang Z, Zhang G. microRNA-106b derived from endothelial cell-secreted extracellular vesicles prevents skin wound healing by inhibiting JMJD3 and RIPK3. J Cell Mol Med. 2021;25:4551–61.
34. Chiu K-H, Karpat M, Hahn J, Chang K-Y, Weber M, Wolf M, et al. Cyclic stretching triggers Cell Orientation and Extracellular Matrix Remodeling in a Periodontal ligament 3D in Vitro Model. Adv Healthc Mater. 2023;12:e2301422.
35. Kamml J, Ke C-Y, Acevedo C, Kammer DS. The influence of AGEs and enzymatic cross-links on the mechanical properties of collagen fibrils. J Mech Behav Biomed Mater. 2023;143:105870.
36. Cavalli G, Heard E. Advances in epigenetics link genetics to the environment and disease. Nature. 2019;571:489–99.
37. Sun H, Gao Y, Ma X, Deng Y, Bi L, Li L. Mechanism and application of feedback loops formed by mechanotransduction and histone modifications. Genes Dis. 2024;11:101061.
38. Fu H-D, Wang B-K, Wan Z-Q, Lin H, Chang M-L, Han G-L. Wnt5a mediated canonical wnt signaling pathway activation in orthodontic tooth movement: possible role in the tension force-induced bone formation. J Mol Histol. 2016;47:455–66.
39. Li Y, Zheng C, Liu Y, He J, Zhang Q, Zhang Y, et al. Inhibition of wnt activity improves peri-implantation development of somatic cell nuclear transfer embryos. Natl Sci Rev. 2023;10:nwad173.
40. Wang S-Q, Liu J, Qin J, Zhu Y, Tin VP-C, Yam JWP, et al. CAMK2A supported tumor initiating cells of lung adenocarcinoma by upregulating SOX2 through EZH2 phosphorylation. Cell Death Dis. 2020;11:410.
41. Ohtani K, Zhao C, Dobreva G, Manavski Y, Kluge B, Braun T, et al. Jmjd3 controls mesodermal and cardiovascular differentiation of embryonic stem cells. Circ Res. 2013;113:856–62.
42. Wei X, Guo J, Li Q, Jia Q, Jing Q, Li Y, et al. Bach1 regulates self-renewal and impedes mesendodermal differentiation of human embryonic stem cells. Sci Adv. 2019;5:eaau7887.
43. Yu J, Virshup DM. Functional regulation of wnt protein through post-translational modifications. Biochem Soc Trans. 2022;50:1797–808.
44. Zhou J, Zhu Y, Ai D, Zhou M, Li H, Li G, et al. Advanced glycation end products impair bone marrow mesenchymal stem cells osteogenesis in periodontitis with diabetes via FTO-mediated N6-methyladenosine modification of sclerostin. J Transl Med. 2023;21:781.
45. Shen C-Y, Lu C-H, Wu C-H, Li K-J, Kuo Y-M, Hsieh S-C, et al. The Development of Maillard Reaction, and Advanced Glycation End product (AGE)-Receptor for AGE (RAGE) signaling inhibitors as Novel therapeutic strategies for patients with AGE-Related diseases. Mol Basel Switz. 2020;25:5591.
46. Jeon S-B, Jeong P-S, Kang H-G, Kim MJ, Yun JH, Lim KS et al. NEK2 plays an essential role in porcine embryonic development by maintaining mitotic division and DNA damage response via the Wnt/β-catenin signalling pathway. Cell Prolif. 2024;e13626.
47. Ding D, Li N, Ge Y, Wu H, Yu J, Qiu W, et al. Current status of superoxide dismutase 2 on oral disease progression by supervision of ROS. Biomed Pharmacother Biomedecine Pharmacother. 2024;175:116605.
48. Ye H, Long Y, Yang J-M, Wu Y-L, Dong L-Y, Zhong Y-B, et al. Curcumin regulates autophagy through SIRT3-SOD2-ROS signaling pathway to improve quadriceps femoris muscle atrophy in KOA rat model. Sci Rep. 2024;14:8176.
49. Yang N, Occean JR, Melters DP, Shi C, Wang L, Stransky S, et al. A hyper-quiescent chromatin state formed during aging is reversed by regeneration. Mol Cell. 2023;83:1659–e167611.
50. Zhang X, Liu L, Yuan X, Wei Y, Wei X. JMJD3 in the regulation of human diseases. Protein Cell. 2019;10:864–82.
51. Nasoni MG, Carloni S, Canonico B, Burattini S, Cesarini E, Papa S, et al. Melatonin reshapes the mitochondrial network and promotes intercellular mitochondrial transfer via tunneling nanotubes after ischemic-like injury in hippocampal HT22 cells. J Pineal Res. 2021;71:e12747.
52. Zurzolo C. Tunneling nanotubes: reshaping connectivity. Curr Opin Cell Biol. 2021;71:139–47.
53. Barutta F, Bellini S, Kimura S, Hase K, Corbetta B, Corbelli A, et al. Protective effect of the tunneling nanotube-TNFAIP2/M-sec system on podocyte autophagy in diabetic nephropathy. Autophagy. 2023;19:505–24.
54. Najeeb S, Siddiqui F, Qasim SB, Khurshid Z, Zohaib S, Zafar MS. Influence of uncontrolled diabetes mellitus on periodontal tissues during orthodontic tooth movement: a systematic review of animal studies. Prog Orthod. 2017;18:5.
55. Mena Laura EE, Cestari TM, Almeida R, Pereira DS, Taga R, Garlet GP, et al. Metformin as an add-on to insulin improves periodontal response during orthodontic tooth movement in type 1 diabetic rats. J Periodontol. 2019;90:920–31.
56. Dorenkamp M, Nasiry M, Semo D, Koch S, Löffler I, Wolf G, et al. Pharmacological targeting of the RAGE-NFκB signalling Axis impedes Monocyte Activation under Diabetic conditions through the repression of SHP-2 tyrosine phosphatase function. Cells. 2023;12:513.
57. Arumugam T, Ramachandran V, Gomez SB, Schmidt AM, Logsdon CD. S100P-derived RAGE antagonistic peptide reduces tumor growth and metastasis. Clin Cancer Res off J Am Assoc Cancer Res. 2012;18:4356–64.
58. Zhang M, Li Y, Rao P, Huang K, Luo D, Cai X, et al. Blockade of receptors of advanced glycation end products ameliorates diabetic osteogenesis of adipose-derived stem cells through DNA methylation and wnt signalling pathway. Cell Prolif. 2018;51:e12471.
59. Wang Q-N, Yan Y-Z, Zhang X-Z, Lv J-X, Nie H-P, Wu J, et al. Rescuing effects of periostin in advanced glycation end-products (AGEs) caused osteogenic and oxidative damage through AGE receptor mediation and DNA methylation of the CALCA promoter. Chem Biol Interact. 2022;354:109835.
60. Long H, Zhang S, Zeng S, Tong Y, Liu J, Liu C, et al. Interaction of RAGE with α-synuclein fibrils mediates inflammatory response of microglia. Cell Rep. 2022;40:111401.


## Publisher's note